Throughput Sensitivity to Antenna Pattern and Orientation in 802.11n Networks

Di Kong, Evangelos Mellios, David Halls, Andrew Nix and Geoffrey Hilton

Centre for Communications Research, University of Bristol, United Kingdom.
Andy.Nix@bristol.ac.uk

Abstract— **In this paper the throughput and packet error rate for an in-home 802.11n network is theoretically derived for two different types of 3x3 antenna configurations. Our first configuration assumes the use of three low directivity omni-directional elements. The second arrangement makes use of three orthogonally orientated directional elements. The spatial and temporal characteristics of the in-home channels are modelled using 3D ray tracing and combined with appropriately orientated complex polarmetric patterns for each antenna element. Physical layer throughput is computed for all modulation and coding schemes using a received bit information rate abstraction technique. The theory shows that directional antennas outperform the omni-directional devices in most cases. Directional elements show increased sensitivity to orientation, however for 83% of locations and orientations they still result in throughput enhancement. Directional antennas provide a 33% improvement in average data rate for random client orientations, improving to 52% with optimum alignment to the multipath.**

Keywords; MIMO, 802.11n, Spatial Multiplexing, Eigen-beamforming, directional antennas.

I. INTRODUCTION

Wireless Local Area Networks (WLANs) are commonly deployed in the home and office. These devices are generally used as a wireless extension to the Internet. The recent high throughput 802.11n extension makes it possible to support higher quality video streaming applications. At present, most video-on-demand applications use the transport control protocol with packet errors resolved via end-to-end retransmission. However, multiple service operators are exploring the viability of streaming high-definition content wirelessly from Set Top Boxes (STBs) to low cost receivers (connected to remote televisions) and portable handhelds (phones and tablets) in the home. These types of application require reliable and robust high throughput wireless links.

The 802.11n WLAN standard was ratified in September 2009 and offers high-throughput modes via the use of multi-input multi-output (MIMO) technology [1]. The standard specifies the use of up to four radio chains in both the access point (AP) and client. First generation 802.11n solutions offered two radio chains and provided peak throughputs of up to 300Mbps at the physical (PHY) layer. Most second generation solutions offer three radio chains with peak rates of up to 450Mbps.

To achieve the headline rates in 802.11n a very high signal to noise ratio is required. Modulation and Coding Scheme (MCS) adaptation is used to match the data rate to the quality of the link. The antennas used at the AP and client influence the perceived channel quality. The data rate at the application layer is reduced by higher layer overheads. For 802.11n the application rate is typically around 60% of the PHY rate.

In order to fully exploit the diversity, spatial multiplexing and array gains available to MIMO systems, the antenna configuration and orientation must be carefully considered. Previous measurements [2] have shown that different antenna configurations and orientations have a significant impact on performance. In this paper the performance of a 3x3 802.11n system is derived for two different types of antenna systems. Firstly, three omni-directional antennas are considered at each end of the link. This is compared with the use of three directional antennas at the AP and client. Our theoretic analysis combines the use of detailed polarmetric antenna patterns, state-of-the-art indoor spatial/temporal ray tracing, and advanced PHY layer simulation for all possible MCS modes. For any location and antenna configuration the model is capable of determining the best MCS mode (comprising the modulation scheme, the coding rate, the number of spatial streams and the use of open or closed loop signaling), and hence the projected throughput. The method is used to compare the use of omni and directional antenna elements in a multi-storey home. Rotation of the client is modelled at each test point to determine the impact of antenna orientation.

II. TEST ENVIRONMENT AND ANTENNA CONFIGURATION

The MIMO channel matrix between the AP and each client is calculated from the spatial convolution of the detailed polarmetric element patterns with the spatial and temporal multipath components from a 3D indoor ray-tracer [3]. This deterministic approach is preferred over the standardized TGn channel model [4] since the latter makes several simplifying assumptions. These include i) simplified angle spread distributions, ii) propagation restricted to the azimuth plane, iii) highly simplified polarization modelling, and iv) no mechanism for modelling specific element patterns [5].

A typical three-floor home is shown in Figure 1. The AP is located on the ground floor and ten client locations are distributed around the property. Analysis is performed at 5.2GHz with 12dBm transmit power assumed per radio chain.

Two multiple antenna array configurations are investigated, as shown in Figure 2. Configuration A uses three ‘idealized’ omni-directional (vertical) elements, while B comprises three ‘idealized’ orthogonally oriented and polarized directional elements that match well to measured patch antennas patterns [2]. The AP and client are assumed to use the same antenna configuration. The AP location and orientation was fixed, however the client was rotated in azimuth (anti-clockwise about the z-axis) in steps of 10^{o}. This

was performed for both antenna configurations and for all ten locations (resulting in 360 test scenarios).

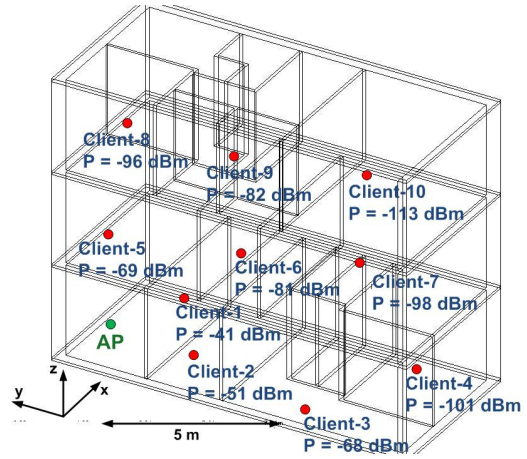

Figure 1. Indoor environment with access-point and client locations.

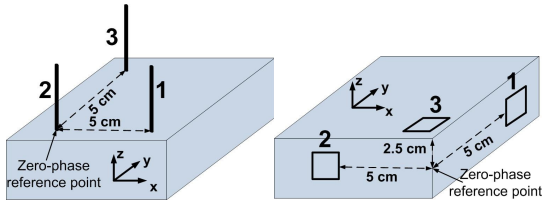

Figure 2. Array configurations; A with omni-directional (left) and B with directional (right) elements (coordinate systems as shown in Figure 1).

For the idealized omni-directional elements, the radiation pattern of a vertically polarized (z-directed) electric current source is assumed (Figure 3) [6]. All power is contained in the vertical polarization and the maximum directivity is 1.8dBi. The half-power points in elevation are +/-45° and the radiation efficiency is modelled at 80% (to take cabling losses and mismatch into account). Figure 1 shows the average received power at all ten locations assuming a single transmit and receive omni-directional element.

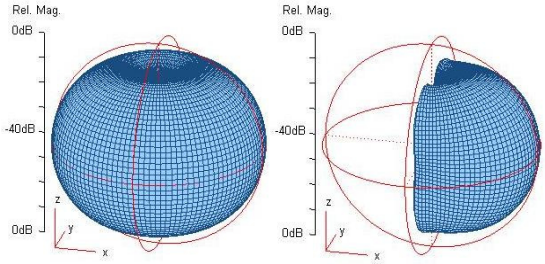

Figure 3. Vertical polarization component of radiation pattern of omni-directional element of configuration A (left) and horizontal polarization component of pattern of directional element 1 of configuration B (right).

For the idealized orthogonally oriented and polarized directional elements of configuration B, two magnetic current sources (z-directed, x-directed and y-directed for elements 1, 2 and 3 respectively) were used to form a beam, radiating only into half space (assuming an infinite ground plane). The efficiency of a directional patch antenna can vary significantly according to the substrate [2]. Measured efficiency values, relative to a high-efficiency monopole, are approximately 40% for FR4 and 80% for RT/Duroid substrate. Hence a radiation efficiency of 50% is assumed. Figure 3 shows the 3D horizontal polarization component of the radiation pattern of element 1. Table I shows the pattern statistics for all the antenna elements of the system.

TABLE I. RADIATION PATTERNS STATISTICS

Element	Power in Polarization (%)		Maximum Directivity (dBi)	
	Vertical	*Horizontal*	*Vertical*	*Horizontal*
Omni-directional	100	0	1.8	-
Directional 1	0	100	-	7.9
Directional 2	84	16	7.9	0.4
Directional 3	57	43	7.9	7.9

In order to compute a statistically valid set of wideband channel matrices suitable for MIMO-OFDM modelling, the procedure reported in [5] was followed. Point-source ray-tracing was performed from the AP to each client location. This provides information on the amplitude, phase, time delay, angle-of-departure (AoD) and angle-of-arrival (AoA) of each multipath component (MPC). The phase of each MPC was adjusted according to the transmitting/receiving antenna's relative distance from a zero-phase reference point (see Figure 2). The complex gain of each MPC was also adjusted according to the transmitting/receiving antenna E-field pattern response for the corresponding AoD/AoA and polarization. The double-directional time-invariant channel impulse response for the m^{th} transmitting and n^{th} receiving antenna link is given by equation (1) [7].

$$h_{mn}(\tau,\Omega_{AoD},\Omega_{AoA}) = \sum_{l=1}^{L} h_{m,n,l}(\tau,\Omega_{AoD},\Omega_{AoA}) = \\ = \sum_{l=1}^{L} \mathbf{E}_l \delta(\tau-\tau_l)\delta(\Omega_{AoD}-\Omega_{AoD,l})\delta(\Omega_{AoA}-\Omega_{AoA,l}) \quad (1)$$

where $\mathbf{E}_l = \begin{bmatrix} E^V_{Tx,m} \\ E^H_{Tx,m} \end{bmatrix}^T \begin{bmatrix} a_l^{VV} e^{j\Phi_l^{VV}} & a_l^{VH} e^{j\Phi_l^{VH}} \\ a_l^{HV} e^{j\Phi_l^{HV}} & a_l^{HH} e^{j\Phi_l^{HH}} \end{bmatrix} \begin{bmatrix} E^V_{Rx,n} \\ E^H_{Rx,n} \end{bmatrix}$

L represents the total number of MPCs. The l^{th} MPC has a complex amplitude $a_l^{XY} e^{j\Phi_l^{XY}}$ (2x2 matrix for all four polarization combinations), a time-of-flight τ_l and departure/arrival angles $\Omega_{AoD,l} / \Omega_{AoA,l}$. $E^{V/H}_{Tx,m} / E^{V/H}_{Rx,n}$ represents the vertical/horizontal polarization component of the m^{th} transmitting and n^{th} receiving antenna E-field radiation pattern. Time-binning was applied, with a bin width of 12.5 ns. The wideband channel frequency response $G_{mn}(f) = [g_{mn1}, g_{mn2}, \ldots, g_{mnN}]$ was computed using a 256-point discrete Fourier transform (equation 2):

$$G_{mn}(f) = F\{h_{mn}\} \quad (2)$$

The 3x3 frequency domain MIMO channel matrix G_k for the k^{th} subcarrier is then calculated as

$$G_k = \begin{bmatrix} g_{11k} & g_{12k} & g_{13k} \\ g_{21k} & g_{22k} & g_{23k} \\ g_{31k} & g_{32k} & g_{33k} \end{bmatrix}. \quad (3)$$

An example of a set of instantaneous wideband frequency responses can be seen in Figure 4 for a 3x3 link. We take 128 (40MHz) or 64 (20MHz) frequency samples to represent the instantaneous wideband channel. To compute the average channel performance for a given location, we repeat this procedure for 1000 channel realizations, applying a uniformly distributed [0,2π] random phase to each MPC.

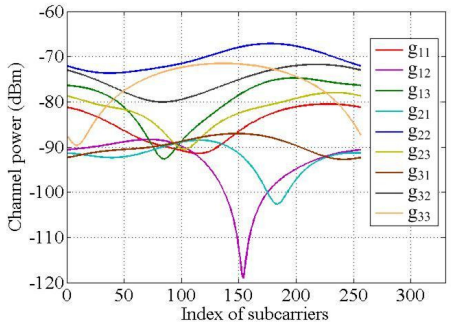

Figure 4. Instantaneous frequency power profile example of a 3x3 MIMO channel (configuration B; location 6; box rotation 210°).

III. Link-Level Abstraction and Validation

Performing link-level analysis for large numbers of locations, MCS modes, antenna configuration and orientations is computationally prohibitive when bit-accurate PHY simulation is applied. To compute these links in an efficient and scaleable manner, a PHY abstraction technique is required. In OFDM systems, where coded blocks are used in the frequency domain, the frequency selectivity from the multipath introduces large SNR variations across the subcarriers. Using a technique known as Effective SNR Mapping (ESM), this SNR vector can be compressed into a single *effective* SNR (ESNR). The ESM PHY abstraction method is described by

$$ESNR = \Phi_m^{-1}\left\{\frac{1}{N \cdot N_{ss}} \sum_{n=1}^{N} \sum_{k=1}^{N_{ss}} \Phi\left(SNR_{n,k}\right)\right\}. \quad (4)$$

$SNR_{n,k}$ represents the post-processing SNR for the k^{th} spatial stream of the n^{th} sub-carrier and m represents the modulation order. N represents the number of sub-carriers in the block, N_{ss} is the maximum number of spatial streams, and $\Phi(\bullet)$ is an invertible function. We use the Mutual Information (MI) ESM approach [7], which defines $\Phi(\bullet)$ as the Symbol Information (SI) as shown in equation (5).

$$SI(\gamma, m) = E_{XY}\left\{\log_2 \frac{P(Y \mid X, \gamma)}{\sum_X P(X) P(Y \mid X, \gamma)}\right\} \quad (5)$$

where Y denotes the received symbol with input SNR equal to γ and $P(Y \mid X, \gamma)$ is the AWGN channel transition probability density conditioned on the noise-free transmit symbol X. $P(X)$ is assumed to be $1/m$. The calculated ESNR is then used to compute the instantaneous PER using a non-faded PER vs SNR look up table (generated via bit accurate simulation for each MCS mode). The ESM PHY abstraction method is fully described in [8] and used extensively in [9].

To verify the accuracy of the RBIR abstraction engine, Figure 5 shows the BER vs SNR performance for three different 2x2 MIMO modes using ½ rate 16QAM. The channel data is based on 1000 frequency domain channel matrix snapshots for location 5. The markers show results from our bit accurate link layer simulator, while the continuous lines were generated from the ESM abstraction model. Excellent agreement can be observed.

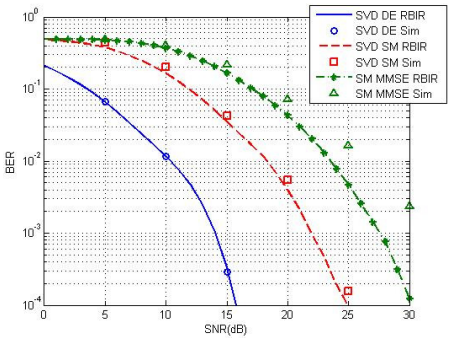

Figure 5. Validation for wideband channel 2x2 MIMO.

Approximately 5 hours of computing time is required to compute just one of the bit accurate graphs shown above (based on a standard dual-core PC). The RBIR ESM abstraction graph was generated in approximately 20 seconds. This vast speed-up allows us to analyse thousands of channels, antenna types, orientations, geometries and polarizations.

IV. Simulation Parameters

Firstly, ten client locations in the three-storey property were selected. For each location, set of 1000 channel snap-shots and antenna orientation, the optimum MCS mode is computed (see Section V-A). The resulting PER and throughput are calculated based on the specific channel data and antenna structures. 1, 2 and 3 stream eigen-beamforming and 3 stream open-loop MMSE models are considered. For each MIMO mode all eight MCS modes are considered, giving a total of $j_{\max}$ =32 possible schemes. The simulation is based on a channel bonded 40MHz transmission and uses 128 sub-carriers (108 active sub-carriers). Peak throughputs of 450, 300 and 150Mbps are achieved for 3, 2 and 1 spatial streams respectively. A noise floor of -93dBm is assumed in the receivers.

V. Results

The PHY layer performance for the three omni-directional antennas is now compared with the directional patch elements. The analysis is based on the ten client locations shown in Figure 1. For each location the client is rotated by 360 degrees in the horizontal plane (to evaluate its sensitivity to orientation). The antenna patterns and polarizations are recomputed as a result of each orientation. To generate a statistically relevant set of results we compute the average throughput and PER over 1000 statistically independent channel realizations. PHY layer throughput is used as the main metric for comparison.

A. Optimum Mode Selection

Table II compares the mean and peak SNR and the mean and peak PHY layer throughput for all ten locations. The clients are orientated at zero degrees and the highest throughput MCS/MIMO mode is chosen (not exceeding a 10% PER threshold) by exhaustive search. For MIMO/MCS mode j (mapping shown in Table III) and client rotation r, the PHY layer throughput $T_{j,r}$ is approximated as

$$T_{j,r} = (1 - PER_{j,r})R_j, \tag{6}$$

where R_j represents peak data rate for mode j. The optimum throughput for rotation r is given by

$$T_r = \max_{j=1:j_{\max},\, PER<0.1} (T_{j,r}). \tag{7}$$

For each location, the mean and peak throughput and the optimum MCS/MIMO mode are given by

$$T_{mean} = \frac{1}{36}\sum_{r=1}^{36} T_r \tag{8}$$

$$T_{peak} = \max_{r=0:10:350} \{T_r\} \tag{9}$$

$$\text{mode} = \underset{j,\, PER<0.1}{\text{argmax}} \{T_{j,r}\}. \tag{10}$$

TABLE II. DIRECTIONAL/OMNI PERFORMANCE AT ALL LOCATIONS

Loc	Mean SNR (dB)	Peak SNR (dB)	Mean Throughput (Mbps)	Peak Throughput (Mbps)	MCS
1	56.4/52.0	60.0/52.0	449.6/447.2	450.0/448.9	24/24
2	47.5/42.4	52.1/42.3	414.4/382.9	446.6/393.4	24/23
3	30.0/24.5	34.4/24.6	213.3/169.7	295.2/175.2	16/13
4	-6.5/-8.3	-4.0/-8.3	None	None	None
5	39.3/23.9	42.5/24.0	363.7/287.4	418.2/291.9	32/16
6	18.3/12.0	21.8/12.0	154.2/86.8	222.1/87.4	14/5
7	-1.1/-5.2	3.8/-5.1	21.0/15.0	57.5/15.0	4/1
8	23.4/-3.1	25.8/-3.0	184.0/15.3	228.5/27.1	14/2
9	16.8/10.6	20.6/10.6	143.4/118.2	257.1/121.8	15/7
10	-4.5/-20.6	-2.6/-20.6	None	None	None

TABLE III. LIST OF MIMO/MCS MODES

	BPSK 1/2	QPSK 1/2	QPSK 3/4	16QAM 1/2	16QAM 3/4	64QAM 1/2	64QAM 3/4	64QAM 5/6
1 Str CL	1	2	3	4	5	6	7	8
2 Str CL	9	10	11	12	13	14	15	16
3 Str CL	17	18	19	20	21	22	23	24
3 Str OL	25	26	27	28	29	30	31	32

Table II summarizes the performance (SNR, throughput and mode) of the omni and directional antenna elements at all ten locations. The mean and peak values were calculated using equations (7) and (8) respectively. The throughputs are based on the optimum MIMO/MCS mode (based on equation 10), which is quoted in the final column (Table III maps the MCS modes to the number of spatial streams, MIMO type, modulation scheme and coding rate).

For locations 1 and 2 (line of sight and closest non line of sight), both antenna systems use the highest throughput closed loop three-stream MIMO mode. However, for some of the harsh locations (positions 4 and 10), the client is unable to associate with either antenna system. For locations 5, 6 and 8, the directional antenna outperforms the omni in terms of mean and peak throughput. In these locations the directional elements support at least two spatial streams, while the omni operates with a single stream. This occurs since the average received signal power is much higher in these locations when directional elements are used. It should be noted that for locations directly above the AP (locations 5 and 8), the directional antennas achieve a much higher SNR than the omni devices since the radiation patterns have a null in the z-direction. For locations 3 and 9, directional antennas provide approximately 33% more throughput (on average) and up to 100% (peak). With the directional elements the peak throughput (at the optimum orientation) is much higher than the average throughput.

From Tables I and II it can be seen that almost all the peak MCS modes are closed loop, with the only exception being for directional antennas at location 5. Closed loop techniques provide transmit array gain, which cannot be achieved in open loop MIMO. In dominant Eigen beam forming, only the strongest Eigen channel is used, which maximizes diversity gain at the expense of multiplexing gain. In SM Eigen beam forming, some or all of the spatial channels are used. This increases the data rate, although high SNR is required in the case of weak spatial channel. As the number of spatial streams is increased, a higher channel SNR and a higher rank matrix channel are required. As a result, closed loop 3x3 MIMO tends to run with three spatial streams in good channel conditions, but only two streams or one stream in poor channel conditions.

B. Impact of Antenna Orientation

Figures 6 and 7 show the predicted throughput for omni and directional antennas at four of the test locations as the client rotates through 360 degrees. Figure 6 shows the average throughput (taken over 1000 independent channel realizations), while Figure 7 shows the instantaneous throughput (based on one specific channel). Results show that the average throughput for omni antennas is insensitive to client orientation; however for the instantaneous channels omni throughput varies with rotation angle [10]. The directional antennas exhibit angular variations for both the average and instantaneous channels. Throughput becomes a function of the directivity of the antenna elements and the spatial clustering of the channel multipath components. Interestingly, in most locations and orientations the throughput observed with the directional elements outperforms the omni devices. The directional elements have greater directivity and better exploit random polarization. Furthermore, since the directional elements illuminate different scattering volumes, the resulting fading is highly uncorrelated. The main disadvantage with directional elements is the potential for strong differences in the mean power (since each element points in a different direction). This is particularly noticeable in channels with low angular spread.

At some locations and orientations (for example, at location 9 from 280 degrees through to 10 degrees) the directional antennas result in performance loss. This occurs since directional antennas can sometimes result in lower signal levels (if misaligned to the significant multipath clusters) and rank deficiency in the spatial auto-correlation matrix (due to power level differences across the elements). Our results show that directional MIMO antennas enhance performance in 83% of cases studied compared to omni antennas.

To better understand the relative performance of the omni and directional antennas, Figure 8 shows the SNR and

determinant of the spatial autocorrelation matrix for all orientations at location 9, as well as the theoretic capacity of the channel. This location was chosen, since as seen in Figure 6, for some angles the average throughout for directional antennas drops below that of the omni devices.

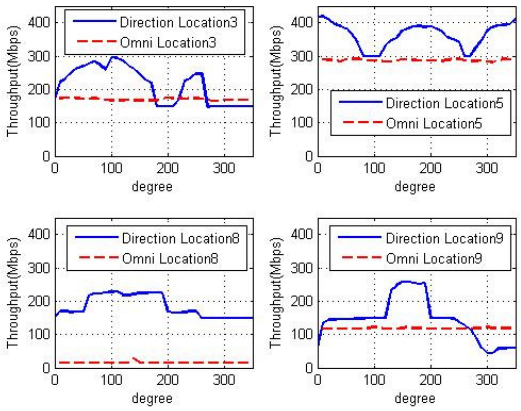

Figure 6. Average directional and omni throughputs (1000 realizations) as clients rotate through 360 degrees at locations 3, 5, 8 and 9.

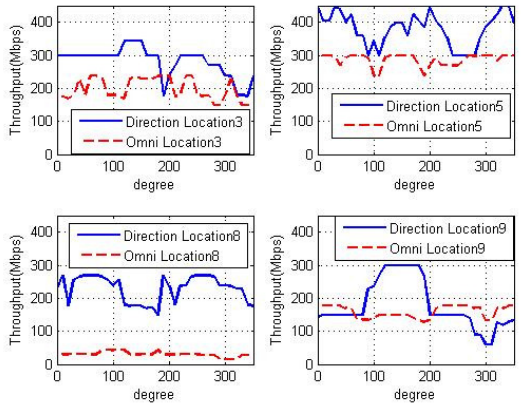

Figure 7. Instantaneous directional and omni throughputs as clients rotate through 360 degrees at locations 3, 5, 8, 9.

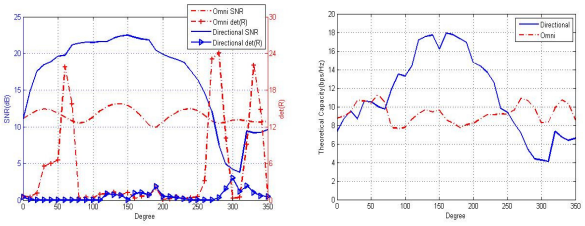

Figure 8. Instantaneous SNR, det(R) (left) and theoretical capacity (right) at location 9.

MIMO channel capacity is known to be a function of SNR and Eigen structure. Figure 8 confirms the drop in directional throughput is a result of reduced SNR. At 280 degrees, the SNR for the directional and omni elements are similar; however the determinant of the omni system is greater, resulting in a higher system throughput. For higher angular rotations, the directional antennas result in reduced SNR, and hence a lower throughput. With directional antennas low spatial correlation is guaranteed, however for channels with low angular spreads the mean power per element can differ significantly, resulting in rank deficiency and the inability to support high numbers of spatial streams. With omni antennas, a similar power level per element is guaranteed, however the spatial fading can become correlated (since each element sees the same set of spatial scatterers), again resulting in a loss of MIMO throughput. Results from all ten test locations show that directional elements outperform omni elements (in terms of higher throughput) at most locations and orientations.

The theoretical capacity curves for location 9 (right-hand graph in Figure 8) follow the trends of the instantaneous throughput shown in the bottom right-hand graph of Figure 7. The peak theoretic capacity (based on SNR and channel matrix values) is 18bps/Hz. Hence, the 300Mbps peak throughput seen at this location represents 42% of the theoretic value.

VI. Conclusions

In this paper the impact of antenna pattern and orientation on 802.11n throughput was theoretically analysed for an in-home environment. Analysis combined site specific ray tracing, polarmetric element patterns and novel RBIR ESM PHY layer abstraction. The average throughput with directional antennas in ten test locations and 36 different orientations was 243 Mbps with random rotation, increasing to 296 Mbps when optimally aligned to the multipath scatter. This compared with 190 Mbps and 195 Mbps respectively for omni-directional antennas. Directional antennas were found to deliver 33% more throughput for random client orientations, increasing to 52% with optimum alignment. On average, omni-directional antennas were insensitive to client orientation, although this was not the case for instantaneous throughput. Directional antennas had increased sensitivity to rotation, however for 83% of locations and orientations they resulted in enhanced exploitation of the available MIMO resources.

References

[1] IEEE 802.11n Working Group, "IEEE Standard for Information Technology-Telecommunications and Information Exchange Between Systems-Local and Metropolitan Area Networks-Specific Requirements-Part 11: Wireless LAN Medium Access Control (MAC) and Physical Layer (PHY) Specification-Amendment 5: Enhancements for Higher Throughput", Sept. 2009.

[2] E. Mellios, G.S. Hilton, and A.R. Nix, 'Optimising radio coverage for wireless media servers,' *Loughborough Antennas and Propagation Conference (LAPC)*, pp.233-236, Nov. 2010.

[3] B.S Lee,.A.R Nix and J.P. McGeehan, 'Indoor space-time propagation modelling using a ray launching technique,' *IEE Antennas and Propagation*, vol.1, pp.279-283, 2001.

[4] TGn Channel Models, IEEE P802.11-03/940r4, May 2004.

[5] Y.Q Bian, A.R. Nix, E.K Tameh and J.P McGeehan, 'MIMO–OFDM WLAN Architectures, Area Coverage, and Link Adaptation for Urban Hotspots,' *IEEE Trans. Veh. Tech*, vol.57, no.4, July 2008.

[6] C.A. Balanis, Antenna theory: Analysis and design, 2nd ed., John Wiley & Sons Inc., pp. 133-143, 1997.

[7] J. Zhuang, L. Jalloul, R. Novak, and J. Park, "IEEE 802.16m Evaluation Methodology Document," IEEE 802.16m-08/004r5, 15 Jan. 2009.

[8] L. Wan, S. Tsai, and M. Almgren, 'A fading-insensitive performance metric for a unified link quality model,' *IEEE WCNC*, April 2006.

[9] D. Halls, A.R. Nix and M.A. Beach, 'System Level Evaluation of UL and DL Interference in OFDMA', to be published in *IEEE WCNC 2011*.

[10] I. Sarris and A.R. Nix, 'Design and Performance Assessment of High-Capacity MIMO Architectures in the Presence of a Line-of-Sight Component,' *IEEE Trans. Veh. Tech,* vol.56, no.4, July 2007.